# Enhanced Adsorption-Catalysis Combination in the Removal of Sulphur from Fuels using Polyoxometalate supported on Amphipathic Hybrid Mesoporous Silica Nanoparticles.

**Josefa Ortiz-Bustos[a], Helena Pérez del Pulgar[a], Yolanda Pérez[a,b]*, Isabel del Hierro[a]***

[a] Departamento de Biología y Geología, Física y Química Inorgánica. Escuela Superior de Ciencias Experimentales y Tecnología. Universidad Rey Juan Carlos, 28933 Móstoles (Madrid), Spain.

[b] Advanced Porous Materials Unit, IMDEA Energy, Av. Ramón de la Sagra 3, 28935, Móstoles, Madrid, Spain.

E-mail: isabel.hierro@urjc.es; yolanda.cortes@urjc.es

## Supplementary Material

## Experimental Section.

The following reactants were acquired from Merck and used as received tetraethylorthosilicate (TEOS) 98 %, poly(ethylene glycol)-block-poly(propylene glycol)-block-poly(ethylene glycol) (Pluronic P123), trimethylamine (4.2 M in ethanol), 3-glycidyloxypropyl)trimethoxysilane, sodium hydroxide, hydrogen peroxide solution 30 % ($H_2O_2$), trimethoxymethylsilane ($MeSi(OMe_3)_3$), hexamethyldisilazane $(Me_3Si)_2NH$) and phenyltriethoxysilane ($PhSi(OEt_3)_3$). Dibenzothiophene was purchased from Sigma Aldrich. Hexadecyltrimethylammonium bromide (CTBA) and phosphomolybdic acid solution ($H_3[PMo_{12}O_{40}]$ 20 % ethanol) were purchased from Acros Organics and used as received. Dodecane ≥ 99.8 % was acquired from Alfa Aesar, 2-propanol from VWR Chemicals and 2-(diphenylphosphino)ethyltriethoxysilane ($PPh_2Et_2Si(OEt_3)_3$) and n-octane from Fluorochem. Nitric and hydrochloric acids were purchased from Scharlau. Toluene, dichloromethane, and ethanol were purchased from SDS and distilled and dried from appropriate drying agents [1].

## Characterization Techniques

X-Ray diffraction (XRD) patterns of the materials were obtained on a Phillips Diffractometer model PW3040/00 X'Pert MPD/MRD at 45 KV and 40 mA, with Cu-Kα radiation (λ=1.5418 Å). The adsorption-desorption isotherms of $N_2$ gas were acquired using a Micromeritics TriStar 3000 analyzer, and based on the adsorption branch, pore size distributions were calculated using the Barret- Joyner-Halenda (BJH) model. Thermogravimetric analysis was carried out using a Star System Mettler Thermobalance and infrared spectra were recorded on a Nicolet-550 FT-IR spectrophotometer (in the region 4000 to 400 $cm^{-1}$) as KBr disks. $^1H$ NMR spectra were recorded on a Varian Mercury FT-400 spectrometer. Structural characterization was completed via transmission electron microscopy (TEM) using a PHILIPS TECNAI-10 electronic microscope operated at 200 kV. The electrochemical studies were recorded with a potentiostat/galvanostat Autolab PGSTAT302 equipped with a FRA32M module for EIS measurements. Modified carbon paste electrodes (MCPE) were used as working electrode and were prepared by mixing graphite (electrochemical quality), the hybrid mesoporous nanospheres and nujol as agglutinant. The mixture was capped in a Teflon electrode with copper electrical connexions. $^{31}P$ MAS NMR spectra were recorded at room temperature on a Bruker Avance III/HD spectrometer and a 4mm double resonance probe at MAS rates of 10 KHz, referenced to external standard of ammonium dihydrogen phosphate at 0.69 ppm. These ones were analyzed by cross polarization and 4096

scans were collected with a recycle delay of 5 s and a contact time of 5 ms. $^{95}$Mo MAS NMR spectra were performed at 26.05 MHz using a Bruker Avance III/HD spectrometer with a wide-bore 9.4 T magnet. The spectra were recorded employing a 4.0 mm low frequency probe at MAS rate of 12 KHz, referenced to the external standard $Mo(CO)_6$ at $\delta$ = -1850 ppm. The sequence used to obtain these spectra was a pulse with spinal 64 decoupling, a recycle delay of 5 s and the number of scans was chosen to achieve a good signal to noise ratio. Zeta potential was measured by suspending the samples in a buffered solution of 1 mg ml$^{-1}$ at pH = 7 and using a Zetasizer Nano ZS Malvern Panalytical. X-ray photoelectron (XPS) spectra were recorded with a SPECS spectrometer equipped with a Phoibos150 MCD analyzer and using a non-monochromatic MgAlα. CASAXPS software was used for spectra treatment and quantification. Last, X-Ray Fluorescence (XRF) spectra were recorded in a Panalytical spectrometer MagiX model. The contact angle was measured with an optic goniometer, ramé-hart instrument.

Table S1. Heteropolyanion content measured by XRF and ICP

| Material | XRF mmol/g | ICP mmol/g |
|---|---|---|
| POM-PPh2-Chol-MSN | 0.22 | 0.18 |
| POM-Ph-Chol-MSN | 0.16 | 0.14 |
| POM-Me-Chol-MSN | 0.2 | 0.17 |

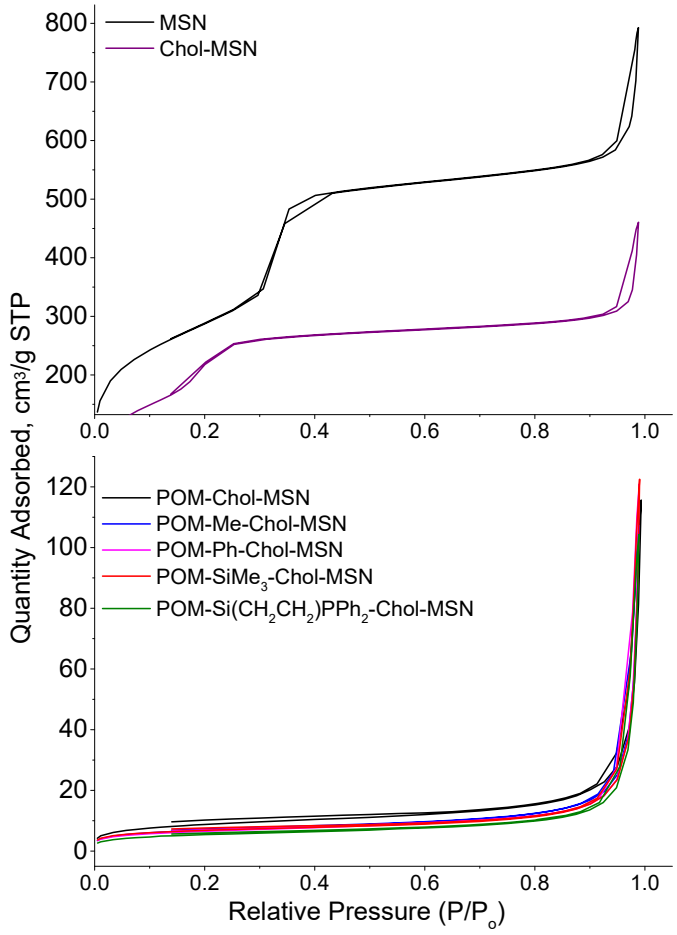


Figure S1. $N_2$ adsorption/desorption isotherms of POM-R-Chol-MSN materials in comparison to pristine Chol-MSN and MSN.

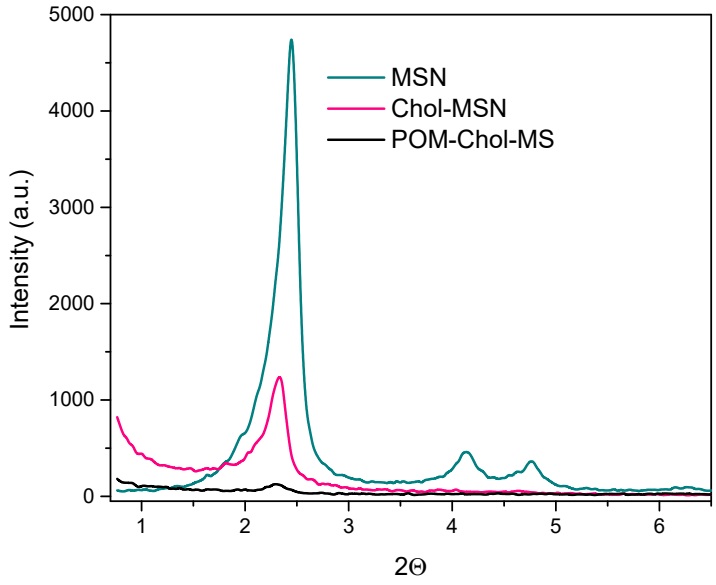


Figure S2. XRD patterns of pristine MSN and hybrid Chol-MSN and POM-Chol-MSN materials.

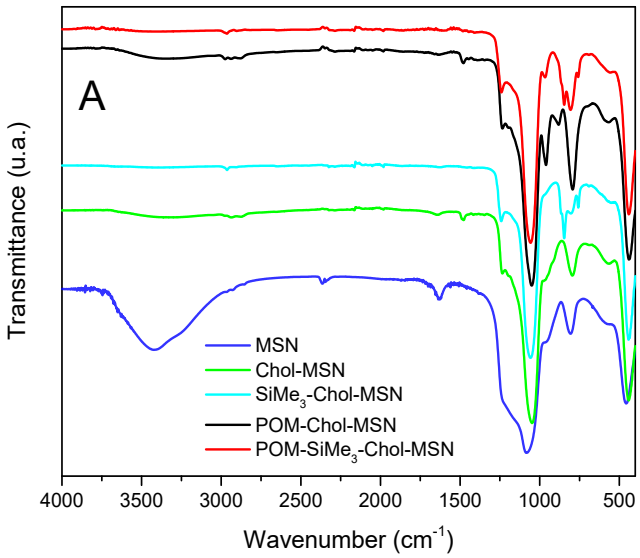

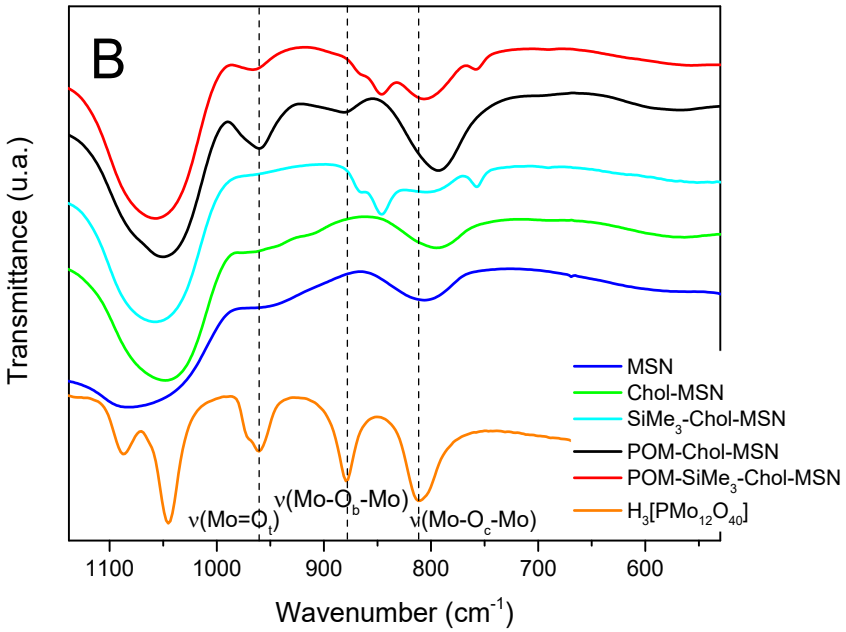


1

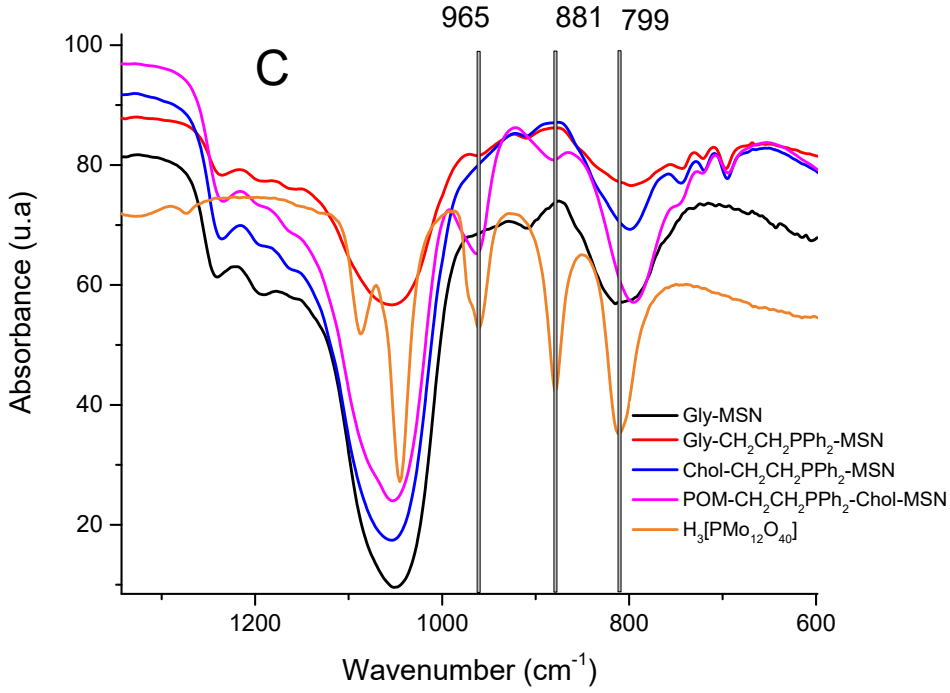


2

3 Figure S3. FTIR step by step in the synthesis of POM-$SiMe_3$-Chol-MSN (A and B) and POM-
4 $SiCH_2CH_2PPh_2$-Chol-MSN (C) as representative materials.

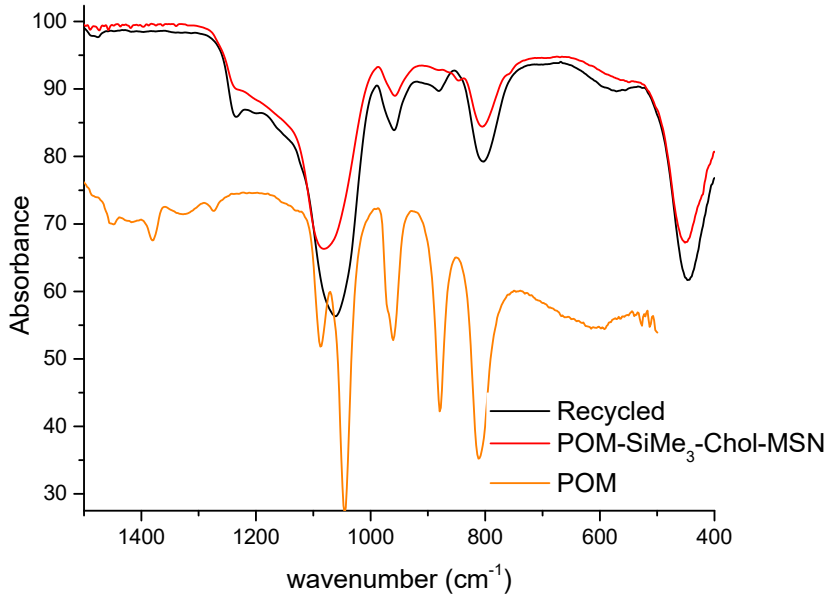


1

2 Figure S4. FTIR of recycled of POM-$SiMe_3$-Chol-MSN after first run.

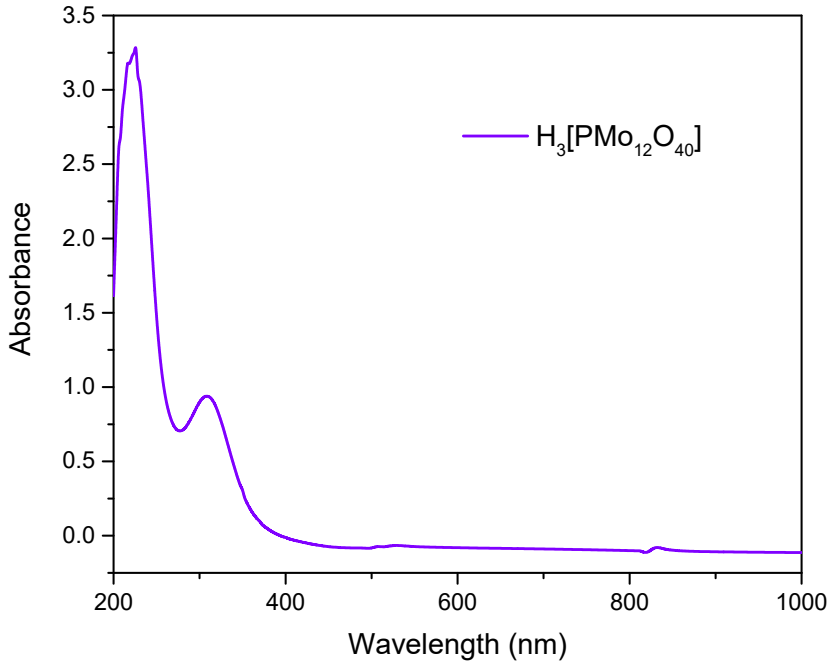


3

4 Figure S5. UV-vis spectrum of phosphomolybdic acid in ethanol, $H_3[PMo_{12}O_{40}]$ at 0.05 mg $mL^{-1}$

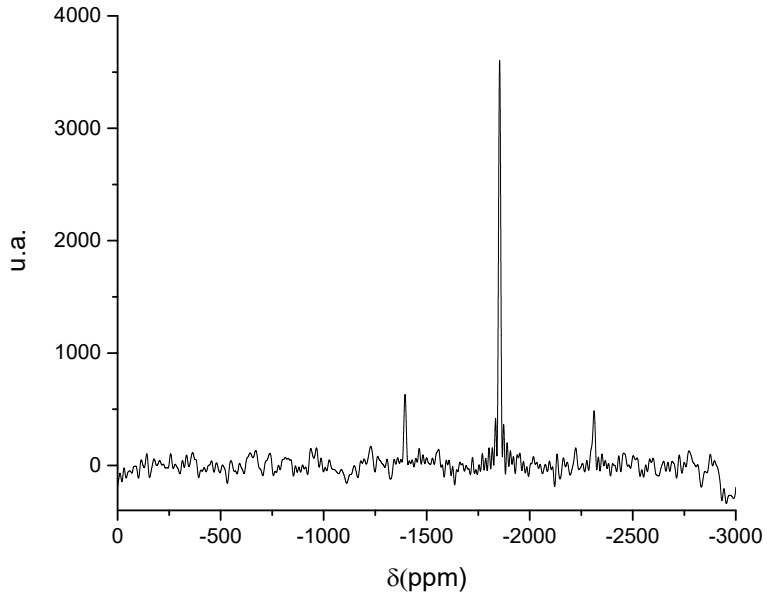


Figure S6. $^{95}$Mo MAS NMR spectra for $Mo(CO)_6$ with $\delta$ = -1850 ppm and line width ($W_{1/2}$) = 0,31 kHz performed at 26.05 MHz at MAS rate of 12 KHz (9,4 T).

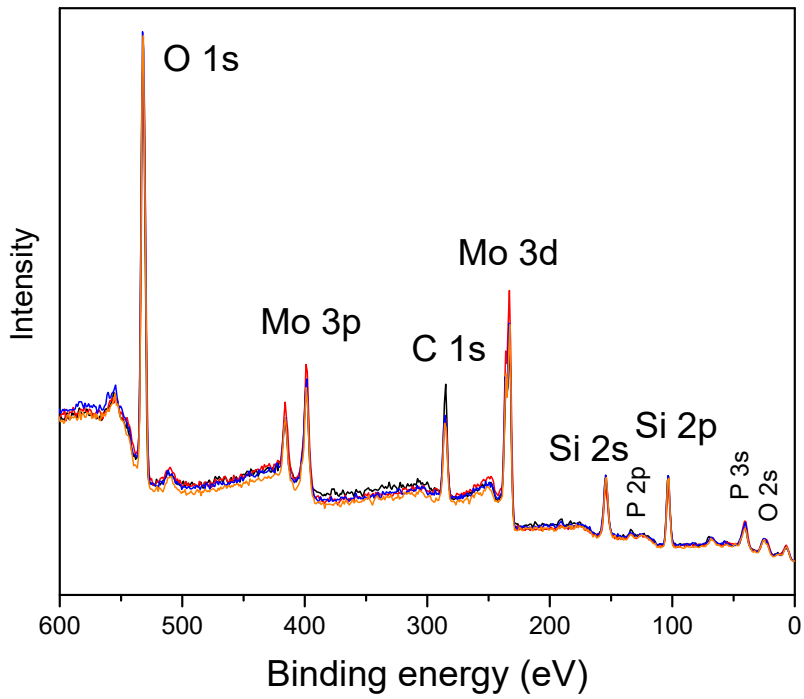


Figure S7. XPS spectra of unsilytated POM-Chol-MSN and silylated POM-R-Chol-MSN materials

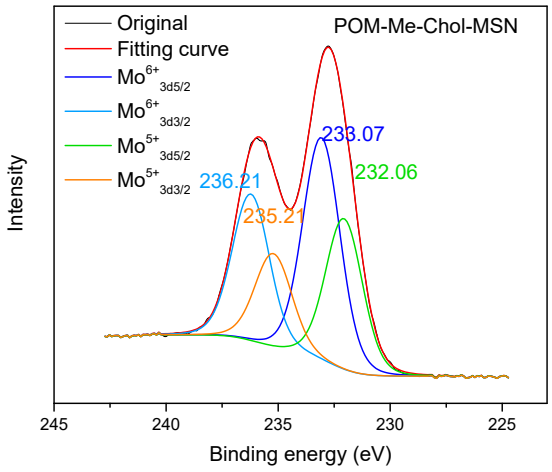


1

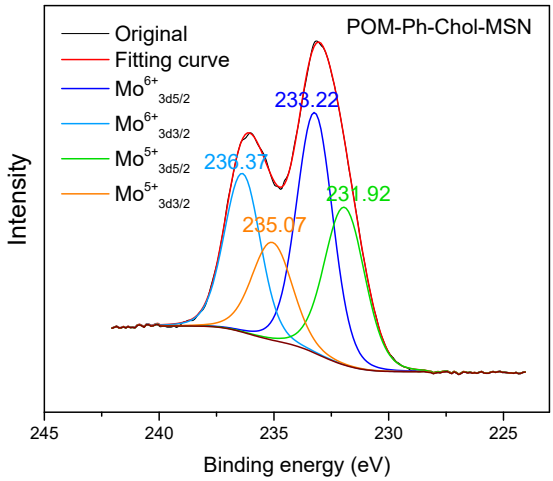


2

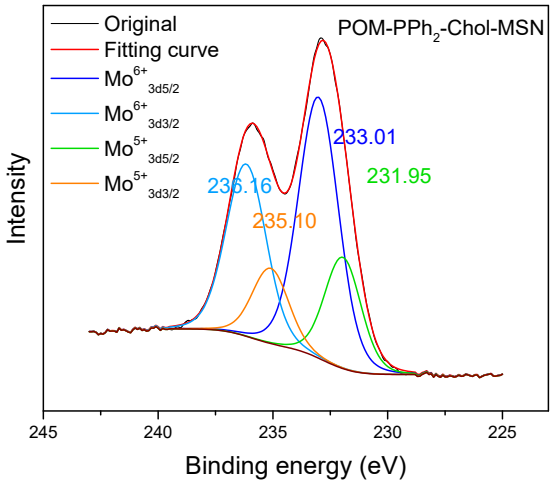


3

4 Figure S8. XPS spectra of Mo 3d silylated POM-R-Chol-MSN materials.

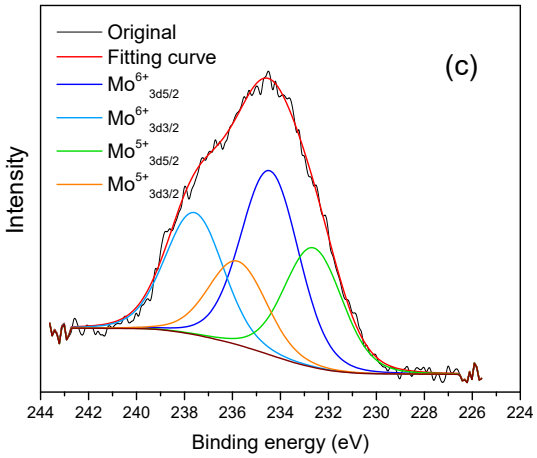


1

2 Figure S9. XPS spectra of Mo 3d recycled POM-Chol-MSN material.

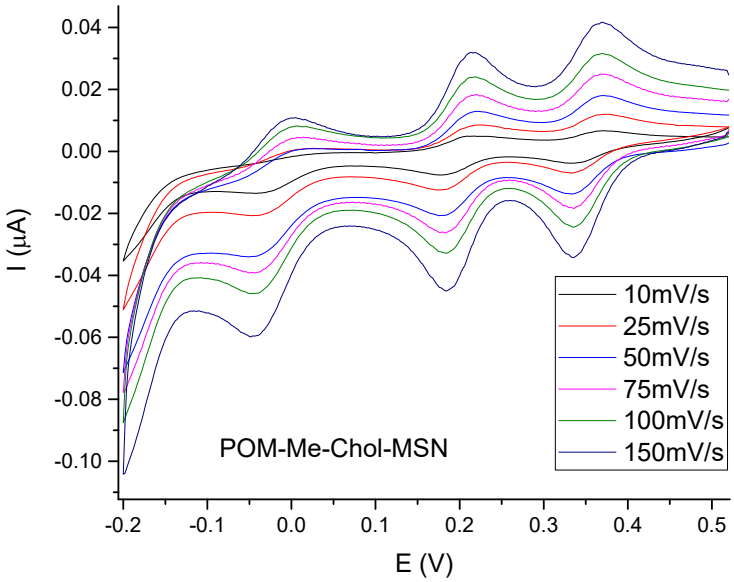


3

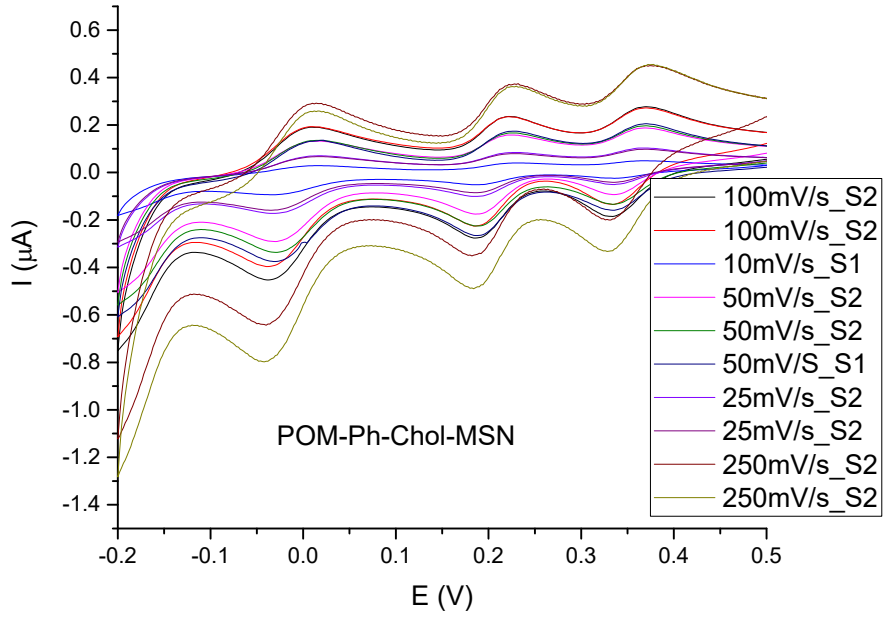


1

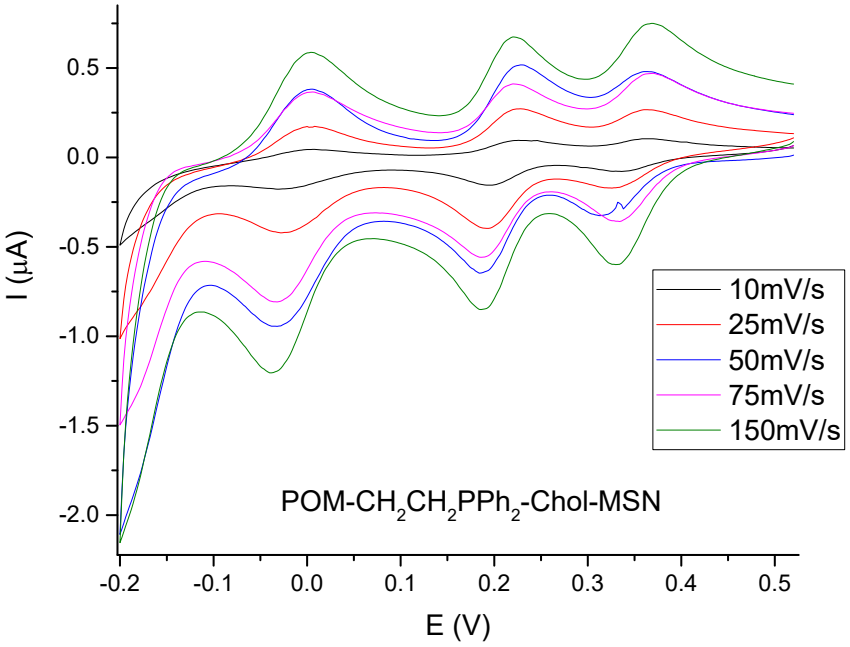


2

3 Figure S10. Cyclic voltammograms of silylated POM-R-Chol-MSN materials immobilized on a
4 carbon modified electrode as working electrode in nitrogen saturated aqueous 0.5 M $H_2SO_4$ vs
5 an Ag/AgCl/KCl (3 M) reference electrode and a platinum rod as counter electrode.

6

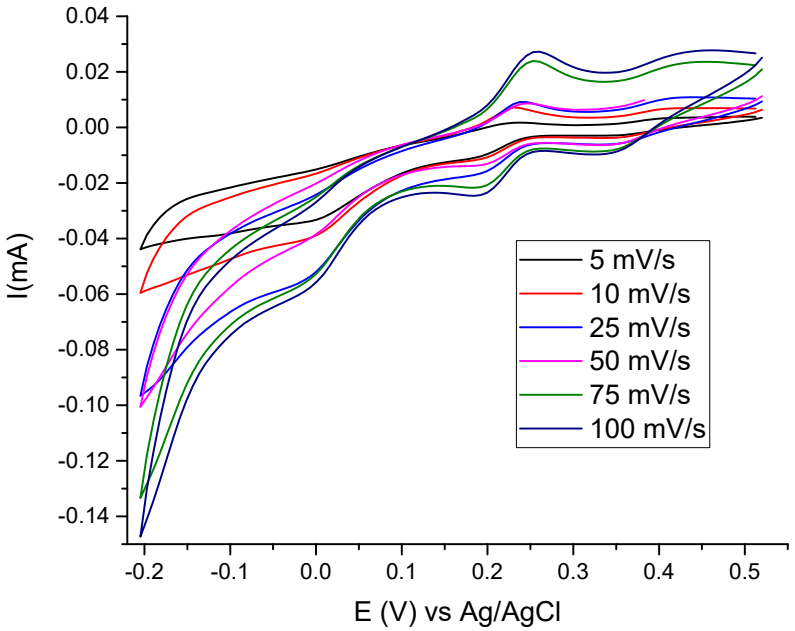


1

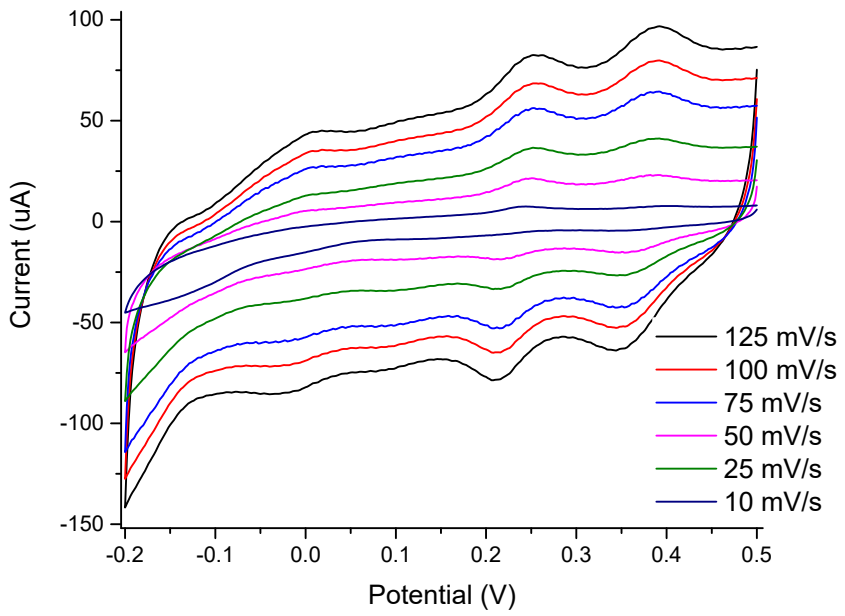


2

3 Figure S11. Cyclic voltammograms of $H_3[PMo_{12}O_{40}]$ using a glassy carbon electrode as working
4 electrode in nitrogen saturated ethanol/aqueous 0.5 M $H_2SO_4$ and aqueous 0.5 M $H_2SO_4$ vs an
5 Ag/AgCl/KCl (3 M) reference electrode and a platinum rod as counter electrode.

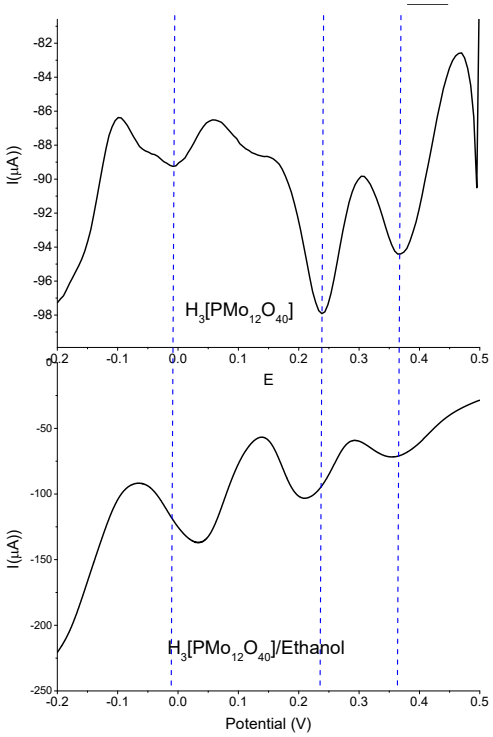


Figure S12. DPV of $H_3[PMo_{12}O_{40}]$ using a glassy carbon electrode as working electrode in nitrogen saturated aqueous 0.5 M $H_2SO_4$ and ethanol/aqueous 0.5 M $H_2SO_4$ vs an Ag/AgCl/KCl (3 M) reference electrode and a platinum rod as counter electrode.

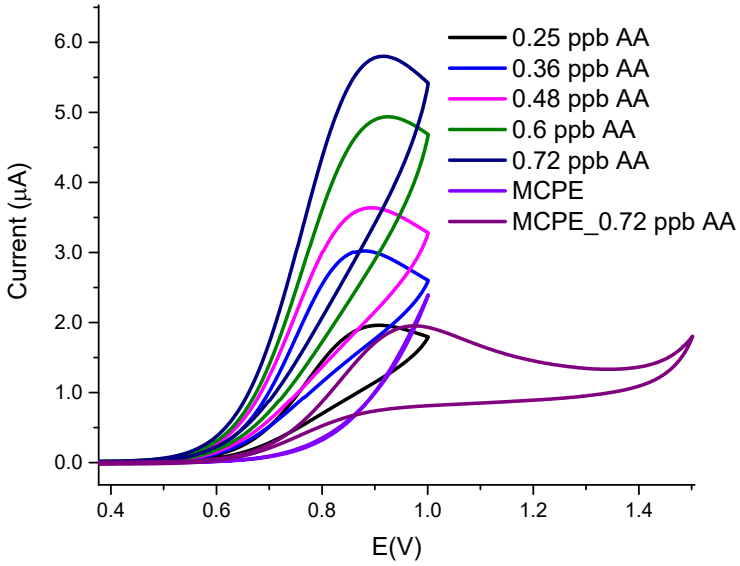


Figure S13. Electrocatalytic oxidation of ascorbic acid by employing POM-$SiMe_3$-Chol-MSN. It is noteworthy that the oxidation peak current of AA appears at lower oxidation potential in the presence of the electrocatalyst and simultaneously the current intensity is enhanced sharply with the increased concentrations of ascorbic acid (AA) in comparison with the modified carbon paste electrode without catalyst (MCPE).

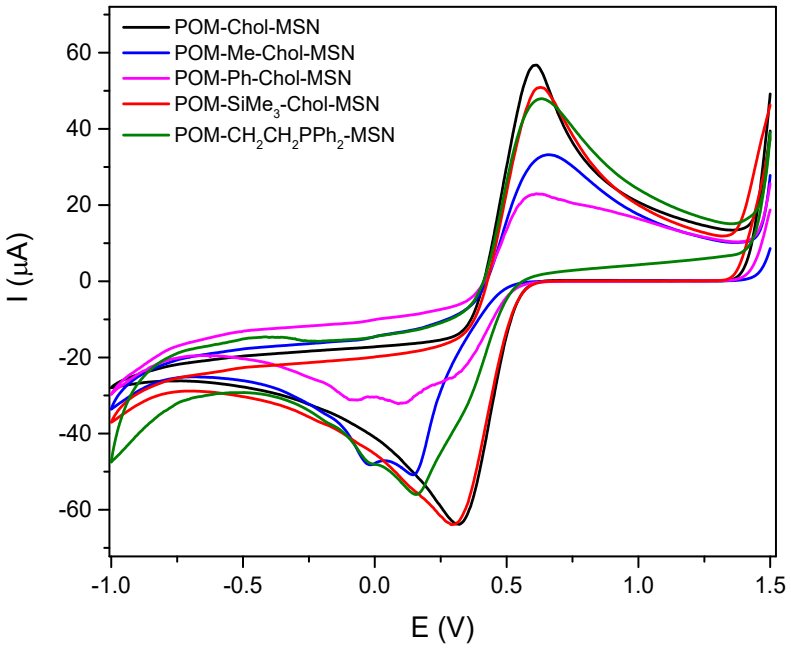


Figure S 14. cyclic voltammograms showing the modification of the materials recorded in 0.5 M $H_2SO_4$ containing the redox system $[Fe(CN)_6]^{3-/4-}$.

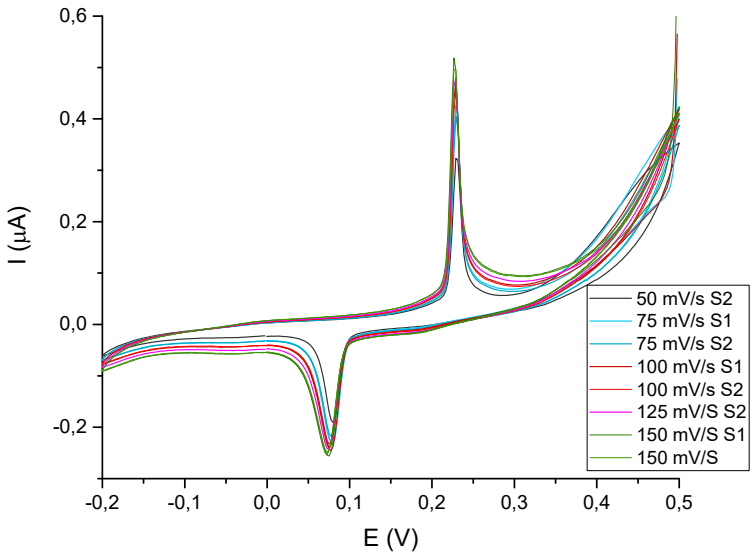


Figure S15. CV of POM-Chol-MSN after two consecutive experiments immobilized on a carbon modified electrode as working electrode in nitrogen saturated aqueous 0.5 M $H_2SO_4$ vs an Ag/AgCl/KCl (3 M) reference electrode and a platinum rod as counter electrode.

Table S2. catalysts based on heterogenized phosphomolybdates for oxidation of DBT in model diesel fuel with $H_2O_2$.

| | **W (wt%)[a]** | **Model oil / co-solvent** | **Catalyst dosage** | **O/S ratio** | **Temperature (ºC)** | **Time (min)** | **Conversion (%)** | **Ref** |
|---|---|---|---|---|---|---|---|---|
| $[Bmim]_3PW_{12}O_{40}$/20% $SiO_2$ | 13 | toluene | 2 g/L | 3 | 50 | 120 | 100 | [2] |
| $(IL)_3PW_{12}O_{40}/SiO_2$ | 2.8 | Diesel | 2 g/L | 36 | 60 | 240 | 92 | [3] |
| $(nBu_4N)_3\{PO_4[WO(O_2)_2]_4\}$ = $(PW_4)$ | 38 | Extractant acetonitrile | 1mM | 7 | 70 | 240 | 97 | [4] |
| $PW_4$@TMA-SBA-15 | - | Extractant acetonitrile | 1mM $(PW_4)$ | 7 | 70 | 240 | 95 | [4] |
| $TBA_3PW_{12}O_4(PW_{12})$ | 63 | n-octane/$BMIPF_6$ | 3µM | 7 | 50 | 60 | 100 | [5] |
| $PW_{12}$@MIL-101 | 38 | n-octane/$BMIPF_6$ | 17 g/L | 7 | 50 | 60 | 98 | [5] |
| HPW/SF-HPC (Hierarchical porous carbons) | 5 | n-octane/methanol | 10 g/L | 10 | 25 | 50 | 100 | [6] |


1 D. B. Williams and M. Lawton, *J. Org. Chem.,* 2010, **75**, 8351-8354 (DOI:10.1021/jo101589h).

2 J. Zhang, A. Wang, Y. Wang, H. Wang and J. Gui, *Chem. Eng. J.,* 2014, **245**, 65-70 (DOI:10.1016/j.cej.2014.01.103).

3 A. A. Bryzhin, M. G. Gantman, A. K. Buryak and I. G. Tarkhanova, *Applied Catalysis B: Environmental,* 2019, **257**, 117938 (DOI:10.1016/j.apcatb.2019.117938).

4 D. Julião, F. Mirante, S. O. Ribeiro, A. C. Gomes, R. Valença, J. C. Ribeiro, M. Pillinger, B. de Castro, I. S. Gonçalves and S. S. Balula, *Fuel,* 2019, **241**, 616-624 (DOI:10.1016/j.fuel.2018.11.095).

5 S. Ribeiro, A. D. S. Barbosa, A. C. Gomes, M. Pillinger, I. S. Gonçalves, L. Cunha-Silva and S. S. Balula, *Fuel Process Technol,* 2013, **116**, 350-357 (DOI:10.1016/j.fuproc.2013.07.011).

6 B. Wang, L. Kang and M. Zhu, *Nanomaterials,* 2021, **11** (DOI:10.3390/nano11092369).